Kontaktlose induktive Strömungstomografie in grundlegender und angewandter Strömungsmechanik

Contactless inductive flow tomography in fundamental and applied fluid dynamics

M. Sieger, R. Mitra, I. Glavinic, S. Sonntag, T. Gundrum, F. Stefani, T. Wondrak, S. Eckert
Helmholtz-Zentrum Dresden-Rossendorf, Institute of Fluid Dynamics, Department Magnetohydrodynamics, Bautzner Landstraße 400, 01328 Dresden, Germany

Strömungsmessung, Flüssigmetall, Tomografie, Inverses Problem, Rayleigh-Bénard
Flow measurement techniques, liquid metal, tomography, inverse problem, Rayleigh-Bénard

Abstract

Contactless Inductive Flow Tomography (CIFT) is a flow measurement technique developed at Helmholtz-Zentrum Dresden-Rossendorf that can reconstruct the global 3D flow field in electrically conducting fluids such as liquid metals. The velocity field of the moving fluid can be reconstructed by solving the underlying inverse problem using appropriate regularization methods. This publication introduces the key concept and mathematical foundation of the method and illustrates the measurement capability of CIFT on two examples: continuous casting of steel in applied fluid dynamics and Rayleigh-Bénard convection as a paradigmatic system in fundamental fluid dynamics.

Introduction

At Helmholtz-Zentrum Dresden-Rossendorf (HZDR), the department Magnetohydrodynamics is engaged in a broad variety of fluid mechanics related research topics including the development of measurement techniques. Contactless Inductive Flow Tomography (CIFT, see e.g. Stefani et al. 2004, Ratajczak et al. 2017) is a promising candidate in the group of inductive measurement procedures. The method is based on measurements of weak magnetic fields produced from a moving conducting liquid under the influence of an applied static magnetic field and the subsequent reconstruction of the global 3D velocity field as will be explained in the first part of this paper. Measurement techniques of non-contact nature allow to probe very hot liquids such as molten steel in continuous casting (CC) or liquid silicon in the Czochralski-growth process. In such processes the opaqueness of the fluid prevents the use of optical methods. CIFT can be used to reconstruct the global flow fields in CC moulds even under the influence of electromagnetic actuators, enabling an online process control to improve the product quality as will be discussed in the second part. Thermally-driven low Prandl number fluids as the eutectic ternary alloy GaInSn show highly turbulent flows (cf. Schindler et al. 2022). Such Rayleigh-Bénard convection studies in the laboratory contribute to a better understanding of turbulent transport processes in geo- and astrophysical systems, which are much too complicated for detailed studies. The opaqueness of the liquid metal prohibits the use of established optical measurement techniques, whereas CIFT proves to be a suitable alternative as will be shown in this paper.

Basic concept of CIFT

In principle, CIFT consists of two distinct steps, being (1) the application of one or several static magnetic field(s) to the conducting liquid and measurement of the flow-induced perturbations that carry the "fingerprint" of the fluid flow and (2) the data analysis, i.e. solution of the inverse problem to reconstruct the velocity field. The first step will be explained in detail in the next paragraph.

The following explanations take particular reference to the schematic CIFT principle in Figure 1: The constant excitation magnetic field $\vec{B}_0$ (in the order of several Millitesla, green arrows) in combination with the thermally-driven flow in a conducting liquid (velocity $\vec{v}$, blue) leads to induced currents (red) according to Ohm's law

$$\vec{j} = (\vec{v} \times \vec{B} - \nabla \varphi) \qquad (1)$$
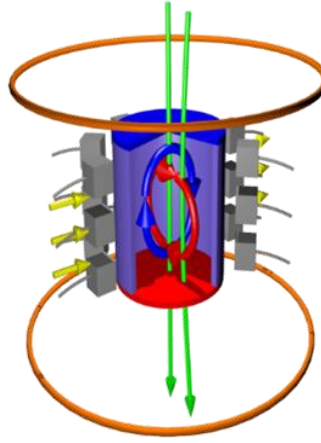
Figure 1: CIFT principle for cylindrical geometry: A pair of coils (brown) produces the excitation magnetic field $\vec{B}_0$ (green), that in combination with the flow of the conducting liquid (blue) leads to induced currents $\vec{j}$ (red). Magnetic fields $\vec{b}$ (yellow) induced from the currents are measured by specific sensors (gray). Here, the fluid flow is driven by a thermal gradient, i.e. heated bottom plate, cooled top plate.

wherein φ is the scalar electric potential. The induced currents $\vec{j}$, in turn, give rise to induced magnetic fields $\vec{b}$ (yellow), which are orders of magnitude smaller than $\vec{B}_0$, usually in the range of Nano- to Microteslas. The precise measurement of such small quantities of magnetic field can be achieved either by (a) Fluxgate coils (usually for a direct current excitation) that are easy to operate but more sensible to changes of the magnetic surrounding of the respective experiment or (b) gradiometric induction coils, developed in-house, see Ratajczak et al. 2016, that are inherently less vulnerable by the use of an alternating excitation current and subsequent frequency filtering and can work close to ferromagnetic parts without problems. Wondrak et al. 2015 give a comprehensive overview on both options. A high-precision power supply and a highly mechanically stable set-up are needed in both cases. To illustrate the difficulties of (sub-)microtesla measurements it is worth mentioning that temperature changes of less than 1 K can lead to relative position changes of sensor to fluid by thermal expansion and contraction which can completely destroy the measurement if no proper care is taken choosing sensor holder materials with low coefficients of thermal expansion, see Sieger et al. 2022a. It should be noted that the strength of $\vec{B}_0$ cannot be chosen arbitrarily: very high values would themselves change the velocity field, i.e. intrinsically corrupt the measurement, while too low excitation fields would lead to immeasurable low induced magnetic fields. In the following paragraph the second step of the CIFT procedure, the reconstruction of the velocity field from the induced magnetic field values, will be explained.

Mathematical basis of CIFT

The flow induced magnetic field $\vec{b}$ is calculated by applying Biot-Savart's law to Equation (1) and solving the emerging Poisson equation for the potential, yielding the following integral equation system valid for low magnetic Reynolds numbers ($R_m < 1$):

$$\vec{b}(\vec{r}) = \frac{\sigma \mu_0}{4\pi} \iiint_V \frac{((\vec{v}(\vec{r}') \times \vec{B}_0(\vec{r}')) \times (\vec{r} - \vec{r}')}{|\vec{r} - \vec{r}'|^3} dV' - \frac{\sigma \mu_0}{4\pi} \oiint_S \varphi(\vec{s}') \frac{\vec{n}(\vec{r}') \times (\vec{r} - \vec{s}')}{|\vec{r} - \vec{s}'|^3} dS' \qquad (2)$$

$$\varphi(\vec{s}) = \frac{1}{4\pi \, p(\vec{s})} \iiint_V \frac{((\vec{v}(\vec{r}') \times \vec{B}_0(\vec{r}')) \cdot (\vec{s} - \vec{r}')}{|\vec{s} - \vec{r}'|^3} dV' - \frac{1}{4\pi \, p(\vec{s})} \oiint_S \varphi(\vec{s}') \frac{\vec{n}(\vec{r}') \cdot (\vec{s} - \vec{s}')}{|\vec{s} - \vec{s}'|^3} dS' \qquad (3)$$

with $S = \partial V$ being the boundary of the fluid volume V. Assuming the boundary being insulating and the conductivity of the liquid σ being homogenous, the induced magnetic field $\vec{b}(\vec{r})$ outside the volume of the fluid under the influence of a primary field $\vec{B}_0(\vec{r})$ can be determined (see Stefani et al. 2004 and Jacobs et al. 2018). The factor p is governed by the shape of the boundary surface and depends on the solid angle at the position $\vec{s}$. The integral equations are solved numerically by discretising V and by employing appropriate shape functions on the resulting elements. For a given number of sensors, this leads to a system of linear equations of the form

$$\tilde{b}(\vec{B}_{0,i}) = M(\vec{B}_{0,i}) \cdot \tilde{v} \tag{4}$$

where the system matrix M and the magnetic flux density $\tilde{b}$ at the sensors are dependent on the excitation magnetic field $\vec{B}_0$. The vector $\tilde{v}$ denotes the velocity field in the discretised volume.

The velocity field can be reconstructed by minimizing the following quadratic functional in $\tilde{v}$:

$$\min_{\tilde{v}}(\textstyle\sum_i \ ||M(\vec{B}_{0,i}) \cdot \tilde{v} - b(\vec{B}_{0,i})||_2^2 + \lambda|A\tilde{v}||_2^2 + \lambda_D|\nabla \cdot \tilde{v}||_2^2)\tag{4}$$

The index i represents the possibility to apply several excitation fields in different directions to get various components of the velocity field. It was shown that two perpendicular magnetic fields are sufficient for a three-dimensional reconstruction as shown by Stefani et al. 2000. Tikhonov regularization is used to mitigate the intrinsic non-uniqueness of the inverse problem and λ represents the regularisation parameter. This parameter allows to trade-off between minimizing the residual deviation of the measured field and minimizing the kinetic energy of the estimated velocity field. λ is determined by the L-curve method using an automated search algorithm to find the second derivatives. The second parameter λ_D is chosen large to ensure the divergence-free condition of the reconstructed velocity. A real-time reconstruction, i.e. flow monitoring, is possible by precomputing the inverse of the linear equation system resulting from Equation (4) for a predefined regularization parameter set.

In this procedure the computation complexity is reduced by replacing Cholesky decomposition to a set of matrix-vector multiplications, which can be carried out in less than one second on a standard CPU [Wondrak et al. 2020, Glavinic et al. 2022a]. Such real-time monitoring of flows is highly relevant for industrial processes as continuous casting of liquid steel [Glavinic et al. 2022b]. Additionally the fast algorithm enables the reconstruction of long measurements that otherwise would produce not manageable large amounts of data.

CIFT in applied fluid dynamics: Flow control in continuous casting

Steel is well-known construction material with an enormous financial turnover. 96% of the 1.82 Mrd. tons are produced by continuous casting (CC). In continuous casting of steel, liquid steel flows from the tundish via a submerged entry nozzle (SEN) into the water-cooled mould where a solid shell is formed at the walls of the mould. This shell with a still liquid core is continuously removed from the bottom of the mould and cooled until it is completely solidified. The flow patterns in the upper part of the mould (cf. Figure 4) are relevant for the quality of the product with regards to surface defects and inclusions [Zhang et al. 2007]. In order to influence the jet leaving the ports of the SEN or the velocity at the meniscus, a variety of electromagnetic actuators were developed in the last decades, including electromagnetic brakes (EMBr), which apply a constant magnetic field in the region of the jet [Cho et al. 2019]. Due to the interaction of the flowing electrically conductive fluid and a strong magnetic field of the EMBr, the fluid will experience Lorentz forces and the flow pattern changes. The strength of the magnetic field is determined by numerical simulations and some plant tests, in which the velocity at the meniscus is usually measured by nail boards and samples of the solidified strand are analysed. In order to be able to directly react to flow instabilities during the casting process, a control of

these actuators based on the current flow structure in the mould would be highly desirable. CIFT in this case proves as a suitable method to circumvent the hindrances of the opaqueness and the high temperature of the melt, to reconstruct the dominating two-dimensional flow structure in a slab casting mould. As several highly ferromagnetic parts come along with the EMBr and other periphery, the use of gradiometric induction coils and an AC excitation current are preferable in this experimental configuration.
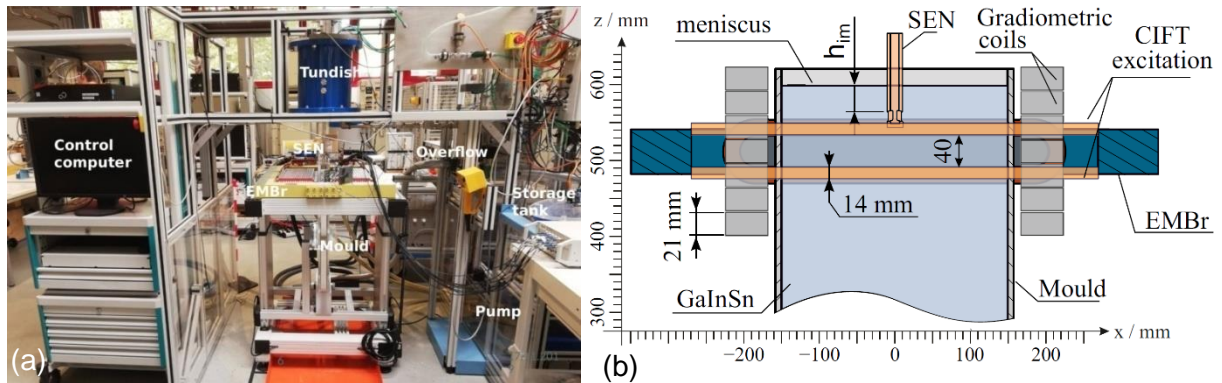
Figure 2: (a) Experimental set-up of HZDR's 1:5 model caster Mini-LIMMCAST. (b) Magnified schematic of the submerged entry nozzle (SEN) region also showing the positions of the CIFT excitation coils and gradiometric coils for measurement and electromagnetic brake (EMBr) positions [Glavinic et al. 2022a].
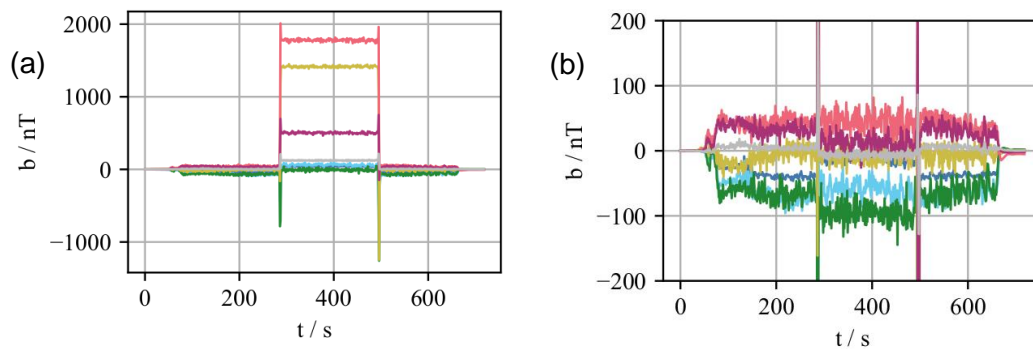
Figure 3: (a) Measurement of the flow-induced magnetic field at the seven gradiometric sensors (cf. Figure 2(b)) for an experiment with an EMBr current of 200 A for t = 290…500 s. (b) Jump compensation by use of a model of the ferromagnetism in the yoke of the EMBr [Glavinic et al. 2022b].

HZDR`s Liquid Metal Model for Continuous Casting (Mini-LIMMCAST) is a 1:5 model of an industrial continuous caster using the ternary eutectic alloy GaInSn as a model fluid for molten steel as it is liquid at room temperature. As in a real caster the liquid metal is poured from the tundish via the SEN into the mould (cf. Figure 2(a) and (b)), that is equipped with an EMBr to influence the direction and velocity of the outgoing liquid stream from the SEN ports, the so-called jet. To reconstruct the mainly 2D flow pattern in the mould with CIFT only one excitation magnetic field is needed. Glavinic et al. 2022a recently showed that it is possible to reconstruct the time dependent flow field in the mould with an active EMBr with a constant strength of up to 400 mT, i.e. two orders of magnitude higher than the actual CIFT excitation magnetic field $\vec{B}_0$. Figure 3 shows a comparison of the actual measured values (Figure 3(a)) of induced magnetic field in the seven gradiometric sensors placed at one of the narrow sides of the mould (cf. Figure 2(b)) under the influence of the EMBr switching on and off at around 290 s respectively 500 s, with the compensated values taking into account the hysteretic ferromagnetism in the yoke of the EMBr (Figure 3(b)). The region of active EMBr now gives reasonable input values for the reconstruction, the remaining spikes are neglected.
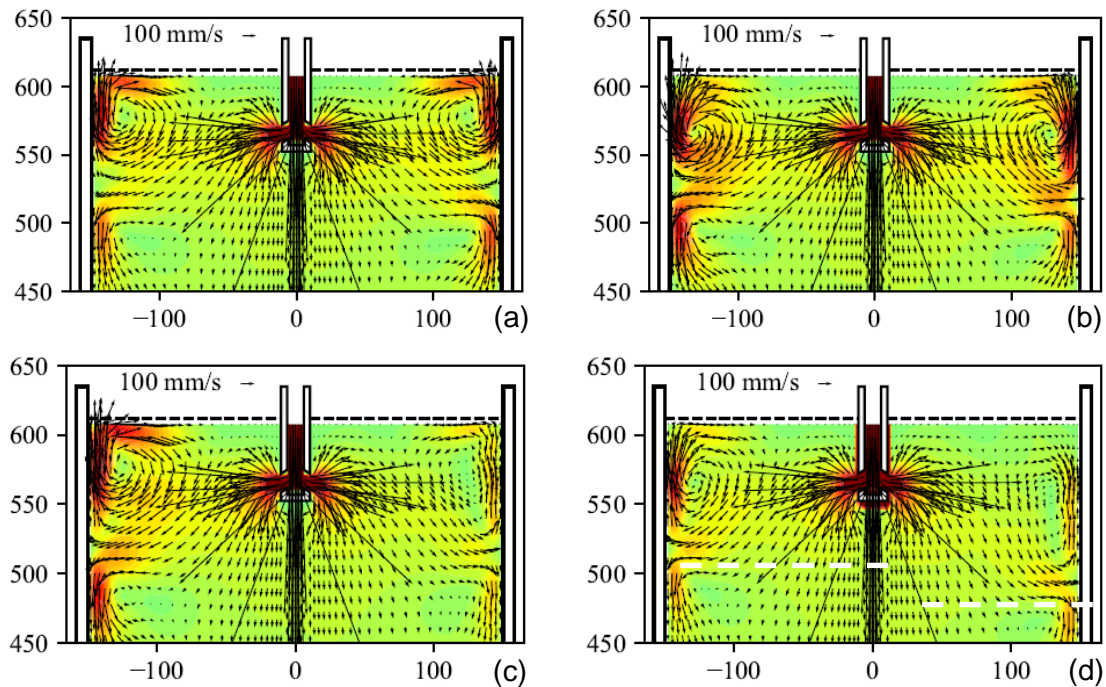
Figure 4: (a) Exemplary flow reconstruction in the x-z-plane of the mould (cf. Figure 2(b)) for different experimental configurations: (a) no clogging, $I_{EMBr} = 0$ A, (b) no clogging, $I_{EMBr} = 200$ A, (c) with clogging, $I_{EMBr} = 0$ A, (d) with clogging, $I_{EMBr} = 200$ A [Glavinic et al. 2022b]. White dashed lines in (d) are a guide-to-the-eye for the uneven jet impingement points induced by the obstacle clogging the right SEN port.

Figure 4 presents four exemplary flow field reconstructions in the x-z-plane, i.e. the same plane as shown in Figure 2(b): while the upper figures represent the reference case of symmetric jets at the left and right outlet of the SEN, the lower plots depict asymmetric flows induced by an artificial obstacle blocking the right SEN outlet port. This configuration is mimicking the important and frequently appearing clogging effects in real casters, leading to lowered velocities at the side of the clogged port and uneven jet impingement points, cf. the white dashed lines in Figure 4(d). CIFT in this scenario is used as a feedback that leads to switching off the EMBr what results in less difference between the left and right jet impingement points. As soon as the obstacle is removed, the control loop again initiates the EMBr. Further details on this CIFT online process control for CC can be found in Glavinic et al. 2022b.

CIFT in fundamental fluid dynamics: Rayleigh-Bénard convection

CIFT is also used to investigate highly turbulent flows in liquid metals driven by a thermal gradient. This Rayleigh-Bénard convection (RBC) [Ahlers et al. 2009] is considered as the classical, sample hydrodynamic paradigm for studying turbulent flows being relevant in geo- and astrophysics. Findings from such laboratory experiments can be compared with phenomena on very different scales by their normalization to certain dimensionless numbers such as Rayleigh or Reynolds number. The choice of model fluid, temperature gradient and the experimental set-up's dimensions offers the possibility to explore the principles of fluid dynamics under very different circumstances.

In particular we investigate thermally driven flows in a liquid metal filled large cylinder with a height of 640 mm and a diameter of 320 mm that is heated from the bottom and cooled from the top. GaInSn serves as the model fluid with a low ratio of kinematic viscosity to thermal conductivity, i.e. low Prandl number in the order of 0.03.

Previous studies of Schindler et al. 2022 identified unexpected regime changes in the heat transport induced by a destabilization of the large-scale circulation with increasing temperature gradient. This study was based on measurements with 19 Ultrasound-Doppler velocimetry (UDV) probes and the obtained velocity fields only provide 2D and 3D flow information in certain crossing points of the measurement lines. To study the global turbulent liquid metal flow fields in more detail CIFT was applied. Large copper coils to produce the excitation magnetic fields in horizontal and vertical direction were mounted to the experiment along with a high number of Fluxgate sensors, see Figure 6. In the current proof-of-concept phase of the experiments only the excitation magnetic field in vertical direction was used, yet a preliminary numerical study proved that even with only one excitation magnetic field sufficiently high correlations of the previously simulated flow field and its numerically treated CIFT counterpart can be achieved. A reference sensor is measuring

Figure 6: Experimental set-up of the large Rayleigh-Bénard experiment at HZDR equipped with 19 Ultrasound-Doppler velocimetry probes, 80 Thermocouples and 42 Fluxgate sensors for CIFT.

changes in the magnetic field surrounding the experiment, e.g. due to severe solar activity, to compensate the small measured values of $\vec{b}$ for such perturbations (cf. Sieger et al. 2022a). First long-term experiments in the order of several hours were carried out with an optimized sensor arrangement, see Mitra et al. 2022, and the vertical excitation magnetic field, to compare the quality of CIFT and UDV. An exemplary result is given in Figure 7(a) that shows a CIFT reconstructed velocity field of a flow driven by a temperature gradient of 1 K at an exemplary time instance. Figure 7(b) gives the according representation by streamlines and shows a 8-shaped structure of the flow, consisting of a slightly smaller upper and a larger bottom roll. The direct comparison of the velocities measured with CIFT along the red line in
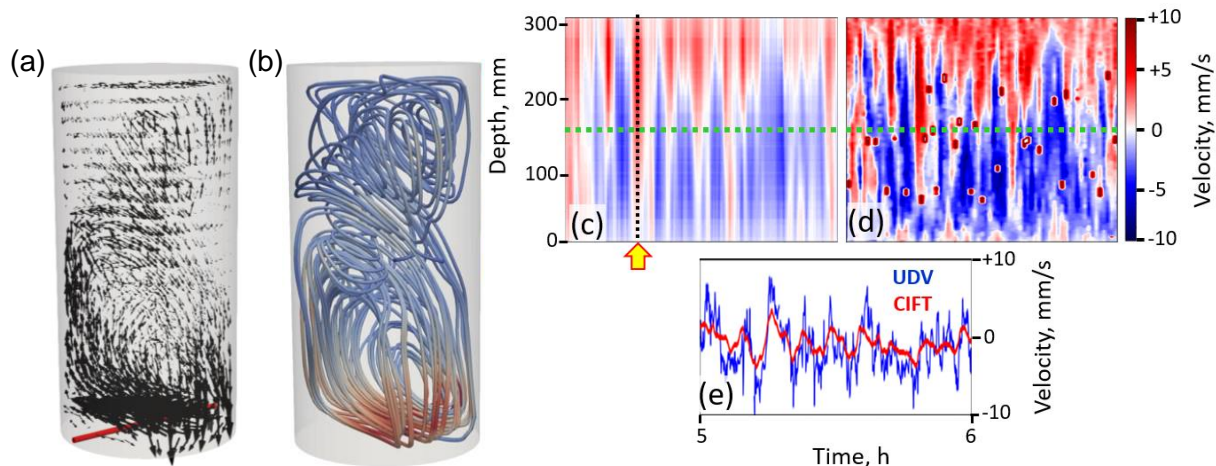
Figure 7: RB experiment with a thermal gradient of 1 K to induce the flow and only the vertical excitation field used, see Sieger et al. 2022b: (a) Experimentally derived CIFT reconstructed global velocity field for a certain time instance and (b) streamline representation of the same velocity field. Velocity profiles measured by (c) CIFT and (d) UDV along the red line marked in (a) for one hour. Green dashed lines indicate the positions of the line-extracts presented in (e). The yellow arrow indicates the time of the 3D-flow field (a). A threshold filter of 10 mm/s was applied to (e), to remove the artifacts present in (d).

Figure 7(a) and its respective UDV counterpart is given in Figure 7(c) for one hour of measurement (x-axis equals time). While the UDV probe intrinsically gives the velocities along its line-of-sight (y-axis equals depth, i.e. diameter), the according information was extracted from the global 3D velocity field measured with CIFT. It is apparent that the shapes of the velocity profiles measured by CIFT and UDV have a very good agreement while the absolute magnitudes are to a certain extent lower for CIFT as the technique intrinsically smoothens out strong local velocity changes. For more details we refer to Sieger et al. 2022b.

Recent experiments could identify a number of different flow structures that might be highly relevant for the heat transfer in RBC cells and are currently under investigation. Figures 8(a) to (c) exemplarily present some distinct structures consisting of one to three rolls in a stacked manner that seem to compete with the predominant chaotic state shown in Figure 8(d).

All experimentally obtained flow fields presented in this paper were obtained from measurements with Fluxgate coils using only one direction of $\vec{B}_0$. The application of both excitation magnetic fields in parallel to increase the quality of the reconstruction even further is not straightforward due to necessary disentanglement of both components in post-processing, which is currently under development.
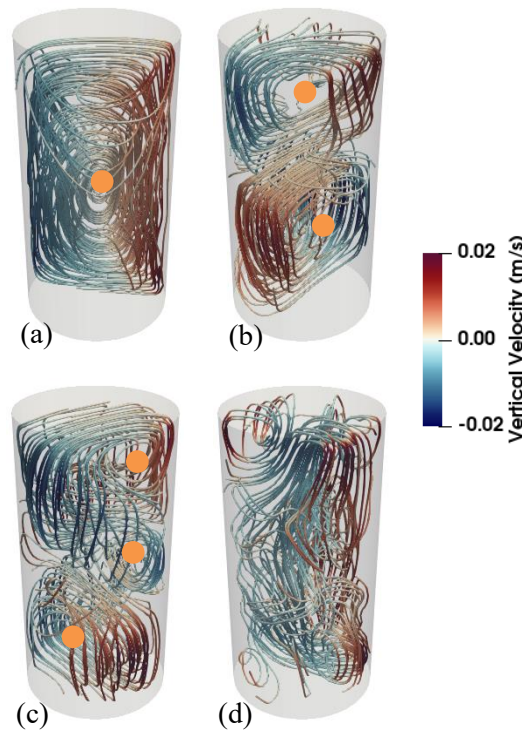
Figure 8: Exemplary flow structures detected in a large cylindrical Rayleigh-Bénard experiment with CIFT: (a) 1-roll-, (b) 2-roll-, (c) 3-roll-structure, (d) chaotic flow field. Velocities are color-coded with respect to the z-direction of the experimental cell, i.e. positive red velocities are directed upwards, negative blue velocities are pointing downwards. Orange dots in (a), (b) and (c) sketch the centers of the according rolls as a guide-to-the-eye.

Conclusions

Contactless inductive flow tomography is a suitable measurement technique for fluid mechanical tasks from fundamental to applied research. The method relies on the precise measurement of very small induced magnetic fields in the order of tens of Nanoteslas till some Microteslas that carry the "fingerprint" of the flow field in electrically conducting liquids. From these datasets the global velocity distribution can be reconstructed by solving the inverse problem, which is possible in less than one second through latest advancements. This fast algorithm gives the possibility to use CIFT as an online process control tool to regulate the strength of electromagnetic brakes and other flow-modifying apparatuses in continuous casting of liquid steel and other metals. With CIFT it is furthermore possible to investigate the global flow field of temperature gradient-driven flows, so-called Rayleigh-Bénard convection, in liquid metals that can act as model experiments for different astro- and geophysical phenomena.

Acknowledgement

References

Ahlers, G., Grossmann, S., Lohse, D., 2009: "Heat transfer and large scale dynamics in turbulent Rayleigh-Bénard convection", Rev. Mod. Phys., Vol. 81, 503

Cho, S.M., Thomas, B.G., 2019: "Electromagnetic forces in continuous casting of steel slabs", Metals, Vol. 9, 471

Glavinic, I., et al., 2022a: "Contactless Inductive Flow Tomography for Real-Time Control of Electromagnetic Actuators in Metal Casting", Sensors, Vol. 22, 4155

Glavinic, I., et al., 2022b: "Laboratory investigation of tomography-controlled continuous steel casting", Sensors, Vol. 22, 2195

Jacobs, R.T., Wondrak, T., Stefani, F., 2018: "Singularity consideration in the integral equations for contactless inductive flow tomography", The International Journal for Computation and Mathematics in Electrical and Electronic Engineering (COMPEL), Vol. 37 (4), 1366-1375

Mitra, R., et al. ,2022: "Optimization of sensor configuration for contactless inductive flow tomography for time dependent flow reconstructions in a Rayleigh-Bénard convection cell of aspect ratio 0.5", Proceedings of The 12th PAMIR International Conference on Fundamental and Applied MHD, 4-8 July 2022, Krakow, Poland

Ratajczak, M., Wondrak, T., Stefani, F., 2016: "A gradiometric version of contactless inductive flow tomography: theory and first applications", Phil. Trans. R. Soc. A, Vol. 374: 20150330

Ratajczak, M., et al., 2017: "Development in the application of contactless inductive flow tomography", Proceedings of the 9th ECCC European Continuous Casting Conference, Viena, Austria

Schindler, F., et al., 2022: "Collapse of coherent large scale flow in strongly turbulent liquid metal convection", Phys. Rev. Letters, Vol. 128, 164501

Sieger, M., et al., 2022a: "Challenges in contactless inductive flow tomography for Rayleigh-Bénard convection cells", Magnetohydrodynamics, Vol. 58 (1), 25-32

Sieger, M., et al., 2022b: "Comparison of contactless inductive flow tomography with ultrasound-doppler velocimetry in a large Rayleigh-Bénard convection cell", Proceedings of the 12th PAMIR International conference on fundamental and applied MHD, 3-8 July 2022, Krakow

Stefani, F., Gerbeth, G., 2000: "A contactless method for velocity reconstructions in electrically conducting fluids", Meas. Sci. Technol., Vol. 11, 758-765

Stefani, F., Gundrum, T., Gerbeth, G., 2004: "Contactless inductive flow tomography", Phys. Rev. E, Vol. 70, 056306

Wondrak, T., et al., 2015: "Increasing Electromagnetic Compatibility of Contactless Inductive Flow Tomography", 2015 IEEE International Symposium on Electromagnetic Compatibility (EMC)

Wondrak, T., Jacobs, R., Faber, P., 2020: "Fast reconstruction algorithm for contactless inductive flow tomography", Proceedings of the 10th International Conference on Advanced Computer Information Technologies 2020, Deggendorf, Germany, 16–18 September 2020; pp. 217–220.

Zhang, T., et al., 2007: "Investigation of fluid flow and steel cleanliness in the continuous casting strand", Metall. Mater. Trans. B, Vol. 38, 63-83